Journal of Manufacturing Processes 125 (2024) 64–74

Contents lists available at ScienceDirect

Journal of Manufacturing Processes

journal homepage: www.elsevier.com/locate/manpro

Research article

Foam additive manufacturing of thermoplastic polymers: The influence of the process parameters

Andrea Lorenzo Henri Sergio Detry [a,1,*], Luca Landolfi [a,b,1], Daniele Tammaro [a], Antonio Lepore [c], Massimiliano Maria Villone [a], Pier Luca Maffettone [a], Antonino Squillace [a]

[a] Department of Chemical Materials and Production Engineering, University of Naples Federico II, Piazzale Vincenzo Tecchio, 80, Napoli, 80125 NA, Italy
[b] Department of Management, Information and Production Engineering, University of Bergamo, Via Pasubio 7B, Dalmine, 24044, BG, Italy
[c] Department of Industrial Engineering, University of Naples Federico II, Piazzale Vincenzo Tecchio, 80, Napoli, 80125 NA, Italy

ARTICLE INFO

Keywords:
Foam additive manufacturing
Composite materials
Polymer foaming
Foam morphology
Soft matter
Material extrusion

ABSTRACT

The widespread adoption of foam additive manufacturing (FAM) in industries ranging from biomedical to aerospace hinges on the precise control of foam morphology, a capability not fully realized with current technologies. This study explores the potential of the FAM process, employing polylactic acid (PLA) and carbon dioxide (CO_2) as a blowing agent, to finely tune the microstructural characteristics of foamed materials through controlled manipulation of process parameters. By systematically varying the pressure of the blowing agent, the time of absorption and desorption, extrusion temperature, speed, and nozzle diameter, we provide a detailed analysis of their individual and collective impact on foam morphology at both macroscopic and microscopic levels. Our findings reveal how specific parameter adjustments can significantly influence the density, diameter, and bubble size distribution within the foamed strands. These insights not only bridge a critical knowledge gap in FAM process optimization but also empower designers and engineers across various sectors to engineer foams with tailored properties for enhanced performance in lightweighting, insulation, and shock absorption applications. This research serves as a foundational guide for advancing the practical utility and scientific understanding of FAM technologies in producing next-generation foamed materials.

1. Introduction

Polymeric cellular materials find many applications, e.g., in the biomedical, engineering, aerospace, nautical, sports, and leisure fields. They possess unique characteristics derived from their morphology, in terms of pore dimensions, orientation, and density [1]. The Nature itself utilizes optimized cellular structures, such as foams, to achieve high performance with minimal material cost [2]. Indeed, natural cellular materials, as, for example, the echinoid and beeswax honeycomb [3], exhibit complex foamed structures that perform specific tasks or optimize particular properties, like the stiffness-to-weight ratio, crash energy absorption, fire resistance, incombustibility, non-toxicity, thermal conductivity, magnetic permeability, and density compared to counterparts without pores. In human bones, the design of cell size and orientation confers them high mechanical properties with minimal weight [4]. Butterfly wings employ foamed structures to optimize energy reflection, again minimizing weight. Scientists often draw inspiration from natural cellular materials for engineering applications, such as lightweight construction, crash energy absorption, noise control, heat exchange, purification, decoration, and arts [5].

Conventional foaming technologies, like extrusion [6] and batch foaming [7], do not allow to control foam morphology locally. According to the available literature, limited attempts have been made to control the local density of foams. Efforts have been made to 3D print polymers into cellular or mesh structures resembling natural cellular materials by stacking extruded strands, where macroscale pores are generated by computer-designed spacing between filamentary struts (inter-strand porosity) [8,9]. However, in those cases, the extruded strands remain densely packed, and achieving cellular structures with micrometric and submicrometric pores is challenging due to the limitations imposed by the nozzle size. Reducing the latter is an inefficient solution for printing cellular materials with submicrometric pores, since it increases the printing time and process costs [5]. Some existing solutions [10,11] to produce foams in additive manufacturing with high inter- and intra-strand porosities involve a two-stage approach: structures with inter-strand macro-porosity are printed in the first step, followed by the production of intra-strand micro-porosity through freeze-drying [12], batch foaming with physical blowing agents [13],

* Corresponding author.
E-mail address: andrea.detry@unina.it (A.L.H.S. Detry).
[1] Authors contributed equally.

https://doi.org/10.1016/j.jmapro.2024.07.015
Received 2 March 2024; Received in revised form 10 May 2024; Accepted 2 July 2024

Table 1
Comparison of foam additive manufacturing technologies.

Technology	Developer	Method	Material used	Key benefits
Direct Foam Writing	Visser et al.	Depositing bubbles one by one	Thermoset polymers	Precise control of foam structure
Vat Photopolymerization	Wirth et al.	Post-printing foaming with CBA	Photopolymers	Consistent morphology after post-processing
Large-Scale Gantry System	Paquet et al.	Layer deposition of polyurethane foam	Polyurethane	Capable of producing large parts quickly
MEX System (FAM)	Tammaro et al.	Two-stage solubilization and extrusion	PLA with CO_2 as PBA	Precise PBA integration, adjustable microstructure, enhanced control over mechanical properties

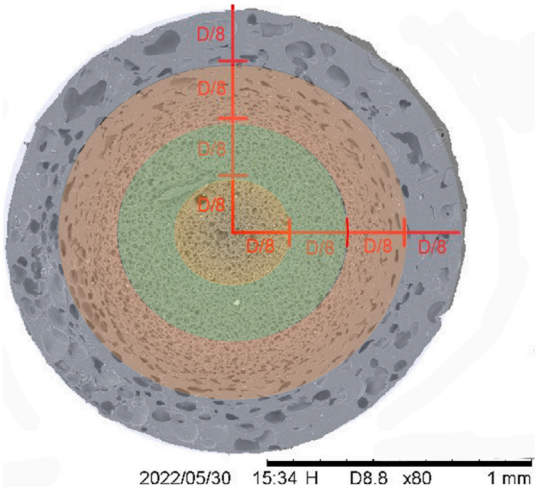

Fig. 1. Example of SEM image of the cross section of a foamed PLA strand with the identification of regions with different foam morphology.

or temperature rise [14]. The two-stage approach necessitates the incorporation of blowing agents directly into the filament, either chemical (CBA) or physical (PBA). While examples employing CBAs for material extrusion foaming exist, as demonstrated by [15,16], such methods often struggle with uneven pore distribution and limited control over pore size and morphology. In the biomedical applications, physical foaming techniques, like gas foaming, are preferred due to their solvent-free nature, absence of chemical reactions, and reduced toxicity when incorporating bioactive species. A recent proposal involves filament foaming in a one-step process using a physical blowing agent into which the filaments are solubilized inline [13]. Although there has been extensive research and interest, the precise relationship between strand cellular morphologies and process parameters in additive manufacturing with foaming remains undefined [17]. Therefore, there is a high demand for intelligent design and control of foam extrusion during 3D printing to address these limitations and establish the relationship between pore structures and process parameters, allowing full use of the design space provided by additive manufacturing of cellular structures [18]. In this paper, the production and characterization of foamed polymeric strands is investigated. The exploration of the parameter space provides informative maps of bubble morphology and distribution in the cross section of the produced foamed strands as a function of the process parameters, such as the blowing agent pressure the time of absorption and desorption the extrusion temperature and speed. As an example, Fig. 1 reports the SEM image of the cross section of a foamed stand, which is characterized by four concentric zones with distinct morphologies. The foam strands considered in this study were produced using polylactic acid (PLA), a biodegradable and biobased polymer that makes the production process sustainable. Carbon dioxide (CO_2) was used as the blowing agent. The established relationships between the process parameters and the foam morphology offer the opportunity to control and optimize cellular distribution and mechanical properties in foam additive manufacturing process.

2. The foam additive manufacturing (FAM) process

In the additive manufacturing field, several technologies have emerged for producing foams. Visser et al. [19] introduced direct foam writing, a technique that enables the creation of thermoset foam structures by depositing bubbles one by one. This method requires precise control over the gas flow and the resin to tailor the foam morphology. In a different approach, Wirth et al. [20] utilized vat photopolymerization printing to manufacture foamed parts, using a liquid photopolymer mixed with a chemical blowing agent (CBA). Their method consists of a post-printing foaming, where the already printed part is placed in an oven and the CBA degrades upon heating, generating gas that forms bubbles, thus resulting in a foam of consistent morphology. Paquet et al. [21] demonstrated the feasibility of depositing layers of polyurethane foam using a large-scale gantry system. This method allows for the rapid production of large parts; however, it results in very rough surface finishes and is limited to the use of a single material. Table 1 provides a summary of alternative technologies for the production of foam in AM.

The foam additive manufacturing (FAM) technique introduced by Tammaro et al. [22] is divided into two main stages, i.e., solubilization and extrusion, as schematized in Fig. 2. During the solubilization, a polymeric filament is positioned within a pressurized vessel, where the physical blowing agent (PBA) is inflated, with precise regulation of the pressure of absorption (P_a) and time of absorption (t_a). This process enables the PBA to dissolve within the polymer, resulting in a polymer/PBA solution. Subsequently, the desorption stage takes place, entailing the storage of the polymeric filament at room pressure and temperature for a defined time of desorption (t_d) before initiating the printing process. In the final stage, namely, extrusion, bubble nucleation occurs, leading to the foam formation. Here, the polymer/PBA solution is pushed into an extruder and experiences rapid pressure drop and temperature rise as it travels through the nozzle, causing the PBA to expand and the polymer to foam. The quick temperature increase and material expansion concurrently aid the crystallization of the foamed polymer.

3. Materials and methods

The process considered in this study is composed of the following phases:

- microbeads selection: this phase involves the selection of suitable PLA microbeads to obtain a filament enhancing foam production;
- filament production: the chosen microbeads are processed through an extruder to create a filament with a diameter $\phi = 1.75$ mm;
- solubilization of the blowing agent: during this phase, the blowing agent (CO_2) is dissolved and distributes into the thermoplastic filament;

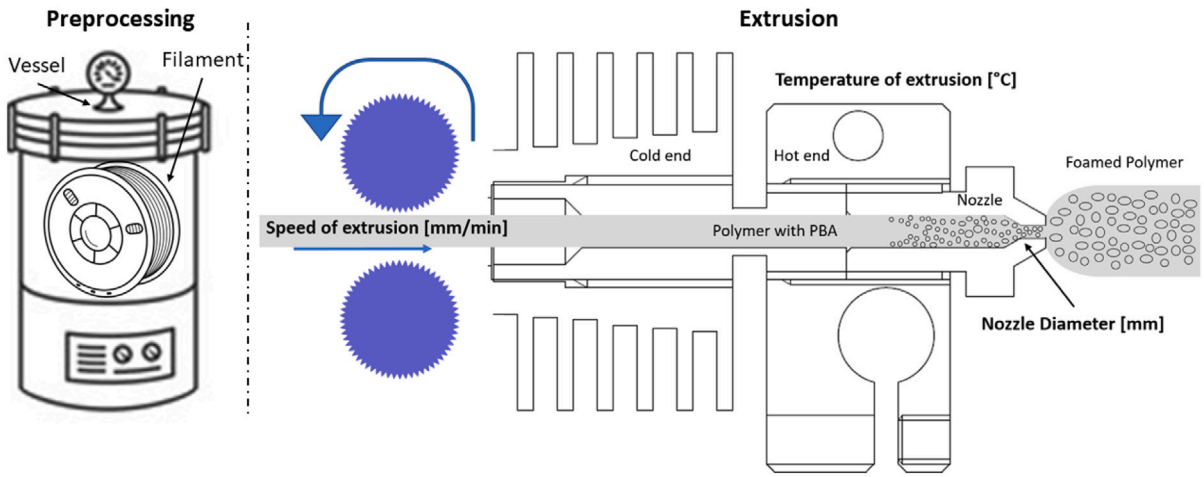

Fig. 2. Outline of the FAM process phases. On the left hand side, a filament spool is positioned inside a pressurized vessel. On the right hand side, the polymer and PBA solution are fed to an extruder, allowing the foaming of the polymer in its nozzle.

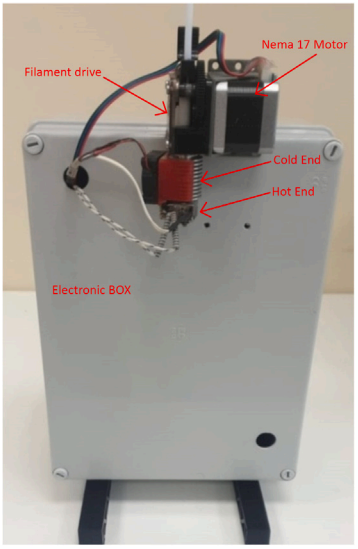

Fig. 3. Photo of the custom made MEX system for producing foam strands using a commercial extruder.

- strand extrusion: the solubilized filament is fed to the nozzle of a 3D printer, where it is extruded and the blowing agent foams, thus creating a foamed strand.

Every foamed strand was analyzed both microscopically, employing microscopy and image processing, and macroscopically, through density and diameter measurements (see Fig. 3).

3.1. Filament production and preprocessing

To achieve high-quality foams, comparable with those obtained in the literature [22], microbeads of PLA with grade 710 M from BewiSynbra (The Netherlands) were used. The PBA chosen for this study is CO_2 with a purity level of 99.95%, sourced from Sol Group S.p.A. (Italy). PLA filaments with a diameter $\phi = 1.75 \pm 0.3$ mm were fabricated thanks to the filament maker 'Composer 350' from 3DEVO (The Netherlands), using the extrusion parameters reported in Table 3.

The filaments produced using the aforementioned process were placed in a specially designed vessel, known as a mini-batch [23]. Carbon dioxide was then introduced into the vessel at room temperature, and the pressure and duration of the solubilization process were carefully controlled to ensure the desired quantity of PBA within each filament. Once the required time had elapsed, the carbon dioxide was safely evacuated using a valve. Subsequently, the filament was extracted from the vessel and stored at room temperature, allowing the carbon dioxide to dissipate from its outer surface. In this phase, the three key process parameters impacting the morphology and properties of the resulting foam are: (i) the pressure of absorption (P_a), namely, the pressure of the PBA during the solubilization process, controlled by an electronic pressure sensor and a pressure regulator; (ii) the time of absorption (t_a), namely, the duration of the solubilization process at pressure P_a; and (iii) the time of desorption (t_d), i.e., the extension of the time during which the filament rests outside the vessel at room pressure and temperature before being extruded.

3.2. Strand extrusion

The filaments containing the PBA were foamed in a MEX extruder 'Titan V6 direct' from E3D (United Kingdom), equipped with brass nozzles of different diameter and controlled by an Arduino-based electronic board with an open-source firmware known as 'Marlin'. The temperature of the extruder was regulated by a proportional–integral–derivative (PID) controller [24], whose parameters are listed in Table 4. An illustration of the MEX setup is provided in Fig. 3, which offers a visual representation of the system's components. The image clearly labels key elements, including the Nema 17 motor that powers the filament drive, the cold end that facilitates filament feeding, and the hot end. Additionally, the electronic control box, which houses the board and the PID controller, is shown.

In particular, the proportional gain (K_p) determines how much the controller responds proportionally to the current error, the integral gain (K_i) determines the controller response based on the accumulation of past errors, and the derivative gain (K_d) predicts the future error and determines the controller response based on its rate of change. The combined effect of these parameters allow to bring the process to its desired set point. The extrusion commands were fed to the apparatus using a host interface program called 'Pronterface'. In this phase, the three key process parameters impacting the morphology and properties of the resulting foam are: (i) the extrusion temperature (T_e), monitored by a sensor located on the hot end of the extruder; (ii) the extrusion speed (S_e), namely, the speed of the filament moving along the extruder, set through the gears that feed the filament to the extruder, and (iii) the nozzle diameter (D_n), namely, the diameter of the final section of the nozzle.

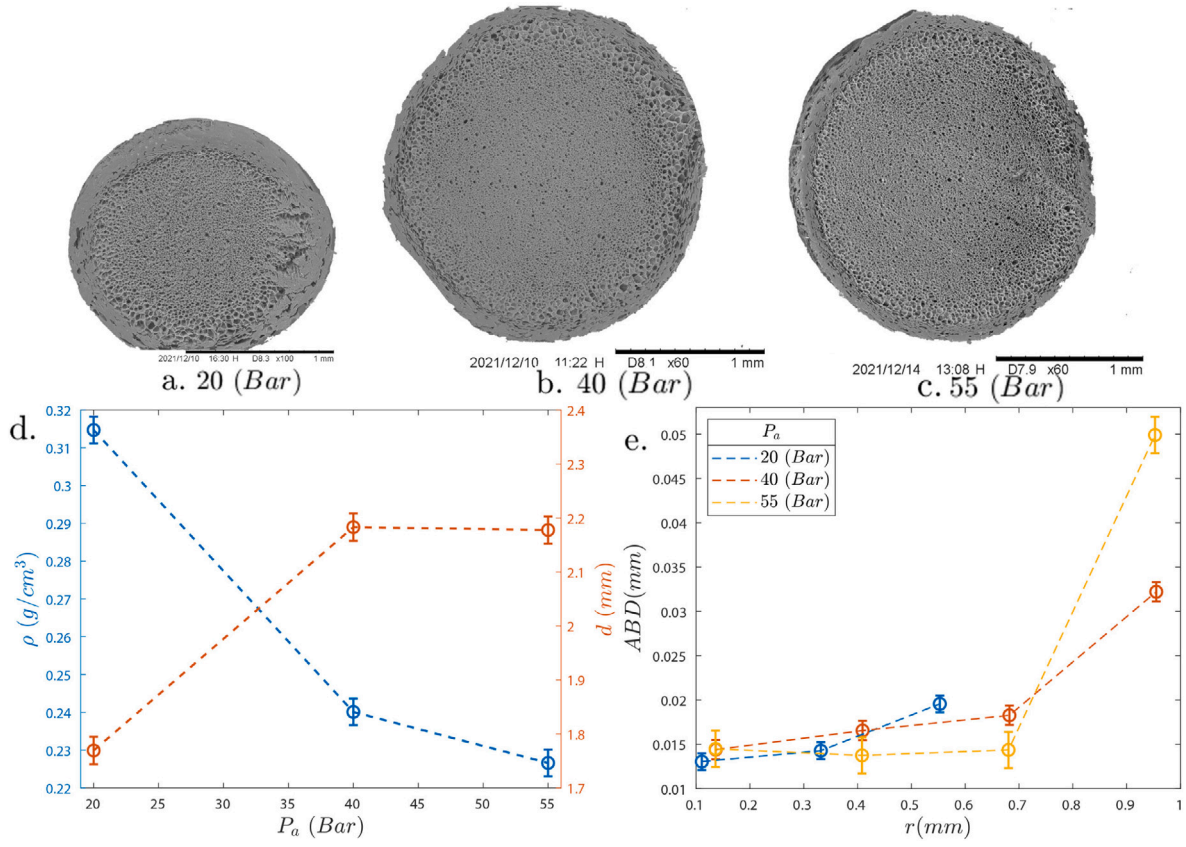

Fig. 4. SEM images of the cross section of strands obtained at $t_a = 71$ h, $t_d = 24$ h, $T_e = 180$ °C, $S_e = 500$ mm min^{-1}, $D_n = 0.8$ mm, and $P_a = 20$ (a), 40 (b), and 55 (c) bar. d: Strand density (blue symbols, see the vertical axis on the left) and diameter (red symbols, see the vertical axis on the right) as a function of the absorption pressure. e: Average bubble dimension along the radius of the strand at the three values of the pressure of absorption considered in the experiments (see legend). In panels d–e, each point is obtained as the average of three measurements; the lines have the scope of guiding the eye. (For interpretation of the references to color in this figure legend, the reader is referred to the web version of this article.)

Table 2
Process parameters and foam property with label and unit of measurement.

Variable	Process parameter	Unit	Symbol	Measured property	Unit
P_a	Pressure of absorption	bar	ρ	Density	g cm^{-3}
t_a	Time of absorption	h			
t_d	Time of desorption	h	d	Strand diameter	mm
T_e	Temperature of extrusion	°C			
S_e	Speed of extrusion	mm min^{-1}	ABD	Average bubble dimension	mm
D_n	Nozzle diameter	mm			

Table 3
Extrusion parameters for filament production.

Description	Value	Unit
Temperature 1	170	°C
Temperature 2	180	°C
Temperature 3	190	°C
Temperature 4	200	°C
Extrusion speed	9	rpm
Fan speed	100	%

Table 4
PID parameters.

Description	Value	Unit
Temperature	200	°C
K_p	22.2	–
K_i	1.08	–
K_d	114	–

3.3. Analysis

Each foamed strand was examined to assess the microscopic foam morphology and to measure quantities such as the strand density and diameter, cell distribution, and the individual cell dimensions. For this analysis, the TM3000 scanning electron microscope (SEM) from Hitachi High-Technologies Corporation (Japan) was utilized, which allows the observation of the distribution of bubbles in the cross section of the strands. The specimens were extracted from the strands, preventively frozen with liquid nitrogen, by cutting them thanks to an Astra Platinum blade. All the analyzed strands were coated with gold by a K650X Sputter Coater from Quorum Technologies (United States) to make them conductive for the SEM analysis. The density of all the strands was measured through the density function of the Gibertini Eternity Scale 300CAL (Italy).

To compute the average bubble dimension (ABD) as a function of the radial coordinate (r) within the cross-section of a strand, an horizontal (or vertical) radius extending from the center to the boundary of the section is considered. This radius is then divided into four equal segments, as illustrated in Fig. 1. Subsequently, the number of bubble walls (N_w) intersecting each segment is calculated. The ratio between

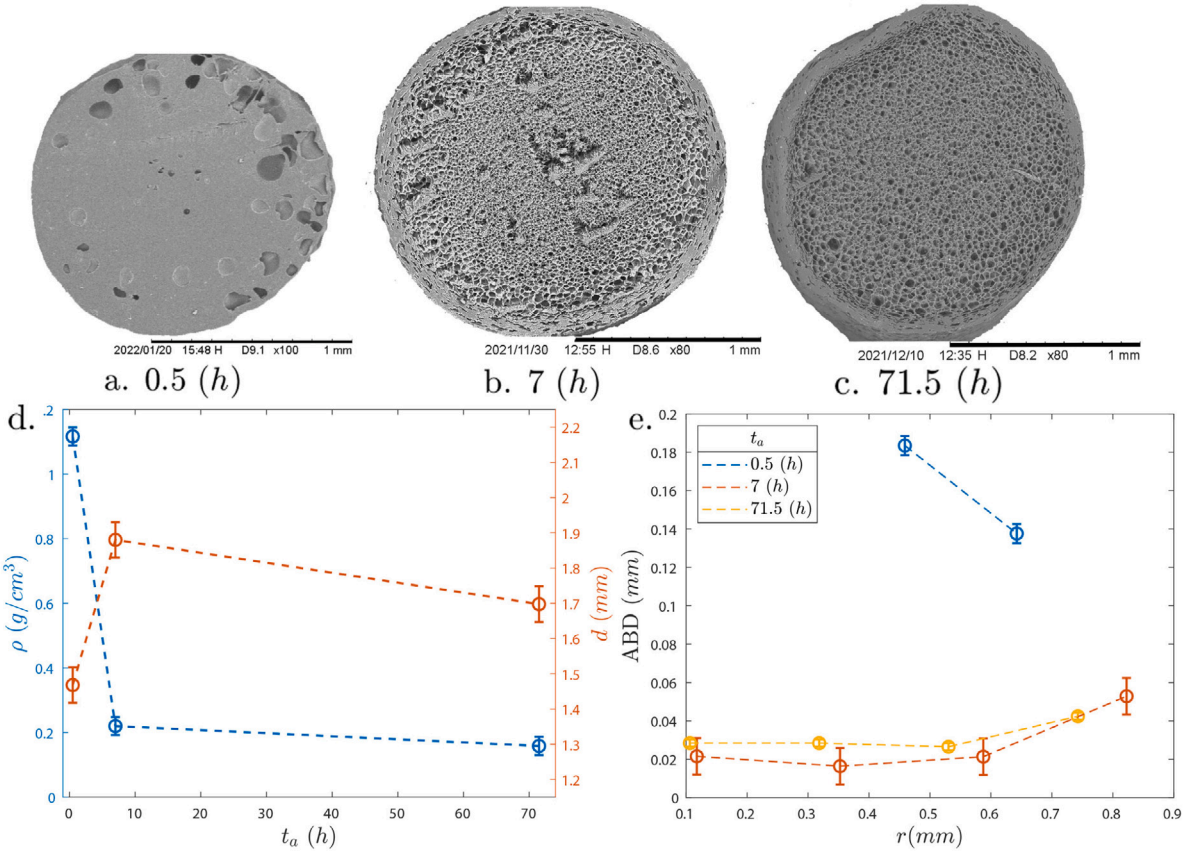

Fig. 5. SEM images of the cross section of strands obtained at P_a = 35.5 bar, t_d = 24 h, T_e = 180 °C, S_e = 500 mm min^{-1}, D_n = 0.8 mm, and t_a = 0.5 (a), 7 (b), and 71.5 (c) h. d: Strand density (blue symbols, see the vertical axis on the left) and diameter (red symbols, see the vertical axis on the right) as a function of the time of absorption. e: Average bubble dimension along the radius of the strand at the three values of the absorption time considered in the experiments (see legend). In panels d–e, each point is obtained as the average of three measurements; the lines have the scope of guiding the eye. (For interpretation of the references to color in this figure legend, the reader is referred to the web version of this article.)

the value of N_w corresponding to a certain segment and the length of the segment (i.e., one fourth of the radius of the strand cross section) yields the average bubble dimension in the annular region to which the segment belongs.

4. Influence of the process parameters

A systematic approach was adopted to investigate the impact of the process parameters on foam morphology and properties. Experiments were conducted by fixing the values of five out of the six parameters and varying the sixth. In what follows, we will show and discuss cross-sectional images that illustrate the impact of each process parameter on foam morphology, in terms of cell size and distribution. Additionally, quantitative data on strand density and diameter and average bubble dimension will be presented, enabling a comprehensive understanding of how the process parameters impact the foam properties. Table 2 presents a comprehensive summary of the process parameters, previously described in the Materials and Methods section and their variables, on the right-hand side of the Table 2, the measured properties of the strands are presented.

4.1. Pressure of absorption (P_a)

The PLA filaments are placed in a vessel with CO_2 at pressure P_a. Since the temperature is kept constant, the quantity of PBA diffusing into the filaments is proportional to P_a [25,26]. Figs. 4a–c show the SEM images of the cross section of strands obtained at P_a = 20 (a), 40 (b), and 55 (c) bar (and at the values of the other process parameters reported in the legend). At the lowest P_a-value, the strand is patently smaller than in the other two cases, where almost the same diameter is observed (see also the red symbols in Fig. 4d). On the other hand, the density of the strand monotonically decreases with P_a (see the blue symbols in Fig. 4d). This phenomenon can be attributed to the desorption of CO_2. This trend can be attributed to variable desorption dynamics. Although the desorption conditions and time are consistent across the samples, the absolute quantity of PBA desorbed is higher for samples subjected to greater pressures due to their increased initial solubility. Consequently, samples saturated at higher pressures experience a relatively larger loss of PBA, which results in a proportionally greater reduction in strand density. This interpretation aligns with the fact that desorption begins at the periphery of the strand, leading to smaller and more densely packed bubbles near the center, while average bubble size (ABS) increases toward the periphery of the strand, as observed across all P_a values in Fig. 4e.

4.2. Time of absorption (t_a)

In the pressurized vessel, the PLA filaments are put in contact with CO_2 for a time equal to t_a. The PBA penetrates the filaments due to mass diffusion [27]. As such transport phenomenon is directed from the periphery to the center of the filaments, their outer regions become saturated with CO_2 more rapidly. If t_a is increased, a deeper diffusion of PBA within the polymer filament occurs. Consequently, t_a determines the amount and the distribution of the PBA solubilized throughout the filaments, which, in turn, influence the growth of the bubbles in the different regions of the cross section of the strands, as displayed in Fig. 5. In particular, Fig. 5a shows that a short t_a = 0.5 h results in the presence of bubbles solely close to the outer surface of the filament,

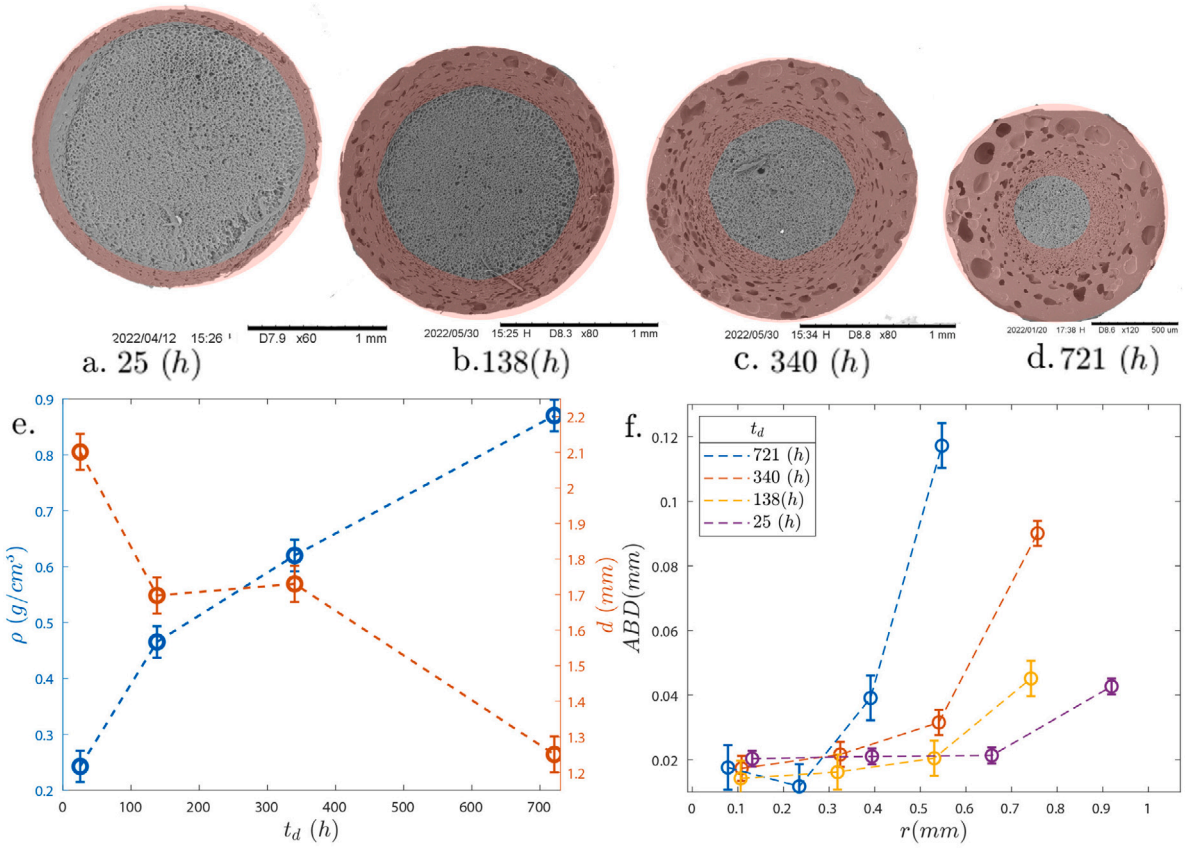

Fig. 6. SEM images of the cross section of strands obtained at $P_a = 32.5$ bar, $t_a = 33$ h, $T_e = 180$ °C, $S_e = 500$ mm min^{-1}, $D_n = 0.8$ mm, and $t_d = 25$ (a), 138 (b), 340 (c), and 721(d) h. e: Strand density (blue symbols, see the vertical axis on the left) and diameter (red symbols, see the vertical axis on the right) as a function of the time of desorption. f: Average bubble dimension along the radius of the strand at the four values of the desorption time considered in the experiments (see legend). In panels e–f, each point is obtained as the average of three measurements; the lines have the scope of guiding the eye. (For interpretation of the references to color in this figure legend, the reader is referred to the web version of this article.)

corresponding to an ABD value of 0 in the inner region of the cross section (see Fig. 5e), whereas Fig. 5d reports that the foam density of the filament with the lowest t_a is comparable to that of bulk PLA (~ 1.25 g cm^{-3}). As t_a increases to 7 h, the PBA completely permeates the cross section of the filament, leading, after the extrusion, to the formation of a cohesive foam structure with a consistently lower density (see Fig. 5b and the blue symbols in Fig. 5d). At the same time, the expansion of CO_2 contributes to an increase in the diameter of the strand (see the red symbols in Fig. 5d). Further increasing t_a to 71.5 h leads to a strand with comparable density, diameter, and ABD profile, as it can be observed by looking at Figs. 5b and 5e. This suggests that, above $t_a = 7$ h, the polymer has reached a state of saturation where, given the temperature, it has absorbed the maximum possible quantity of PBA, thus, increasing t_a has no effect on the foam properties.

4.3. Time of desorption (t_d)

The parameter t_d represents the time between the opening of the pressurized vessel and the start of the printing process, corresponding to a period during which the polymer is stored under ambient conditions. At the beginning of such period, the concentration of the PBA in the strand is higher than that of the surrounding environment, the amount of PBA within the polymer depending on P_a and t_a, as discussed above. As the system returns to ambient conditions, the PBA gradually desorbs from the polymer matrix and diffuses out of it under the action of the concentration gradient, as stated by the Fick's law [27]. Figs. 6a–d show that, as the time of desorption increases, the concentration gradient of the PBA in the cross section of the strand correspondingly increases, leading to a bubble size radial gradient. Also, increasing

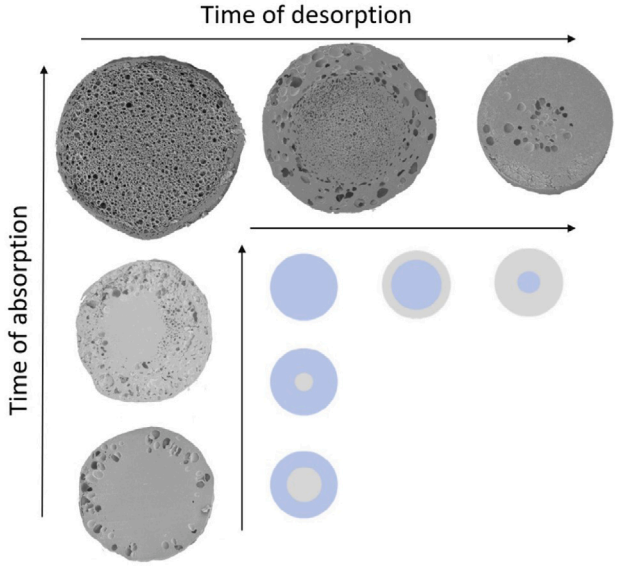

Fig. 7. SEM images of the cross section of strands resuming the overall combined effect of t_a and t_d (given the same values of the other parameters) on foam morphology.

t_d results in a decrease in the overall PBA concentration within the filament, which, from a macroscopic point of view, leads to an increase in the strand density and a reduction in the strand diameter (see

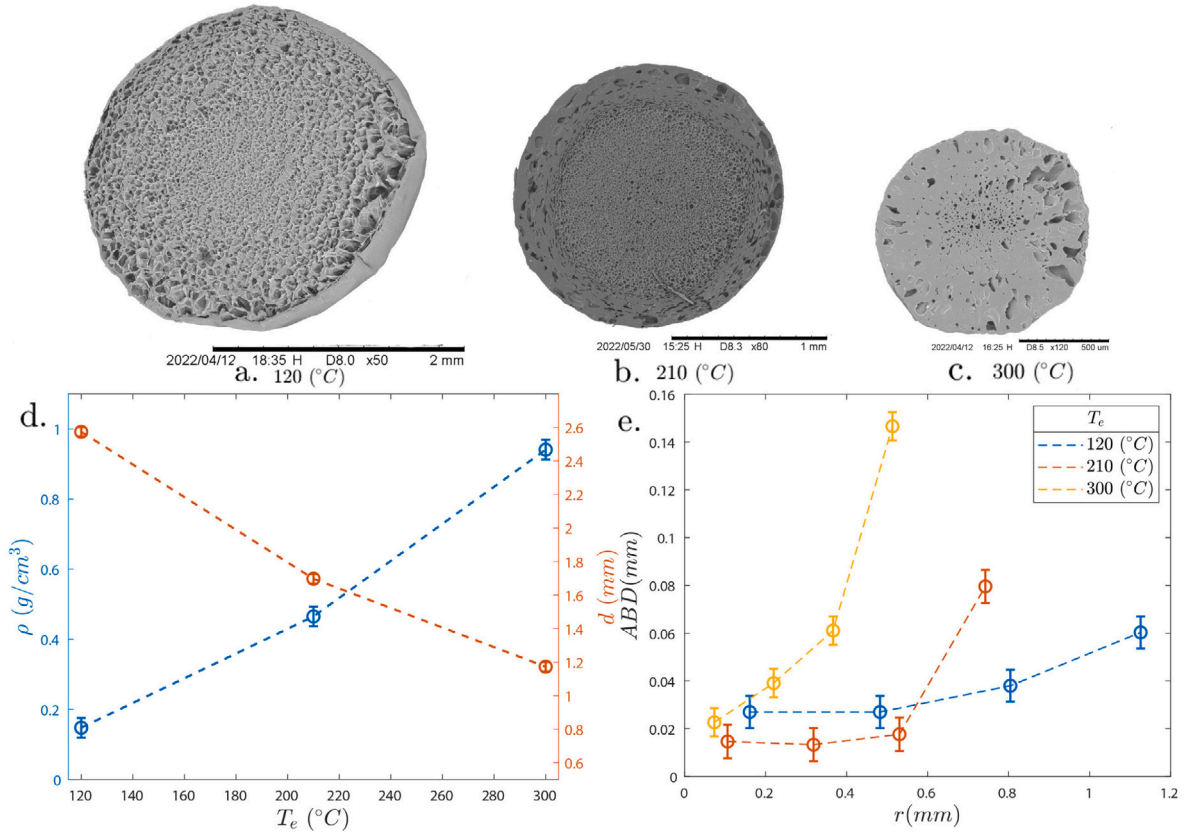

Fig. 8. SEM images of the cross section of strands obtained at P_a = 32.5 bar, t_a = 33 h, t_d = 138 h, S_e = 675 mm min^{-1}, D_n = 0.7 mm, T_e = 120(a), 210 (b), and 300 °C. d: Strand density (blue symbols, see the vertical axis on the left) and diameter (red symbols, see the vertical axis on the right) as a function of the extrusion temperature. e: Average bubble dimension along the radius of the strand at the three values of the temperature of extrusion considered in the experiments (see legend). In panels d–e, each point is obtained as the average of three measurements; the lines have the scope of guiding the eye. (For interpretation of the references to color in this figure legend, the reader is referred to the web version of this article.)

Fig. 6e). By looking at the ABD profiles, it is noteworthy that, at t_d = 340 and 721 h, the ABD in the strand peripheral region exceeds 0.1 mm, which is one order of magnitude larger than the ABD in the core.

Fig. 7 resumes the combined influence of the absorption and desorption times on foam morphology. In particular, t_a plays a critical role in controlling bubble formation in the central region of the strand cross section: increasing t_a promotes a more uniform distribution of the bubbles throughout the strand cross section. On the other hand, t_d governs bubble formation in the outer part of the strand cross section: by extending it, the peripheral region of the strand cross section can empty of the PBA, thus resulting unfoamed after the extrusion. Therefore, properly tuning t_a and t_d offers opportunities for tailoring the strand surface properties to meet specific application requirements, for example in terms of mechanical strength and bonding characteristics.

4.4. Temperature of extrusion (T_e)

The extrusion phase is the part of the foaming process where the nucleation of the PBA takes place in the polymer melt [28] and bubbles are generated, thus T_e plays a crucial role in the FAM technology. Given the other parameters, an increase in the extrusion temperature leads to a decrease in the polymer viscosity, so the nozzle pressure decreases [29]. Obtaining a low-density foam does not merely require maximizing the pressure difference between the inside and outside of the nozzle by reducing T_e to the lowest possible value. While a lower T_e can increase this pressure difference, it can also significantly increase the polymer viscosity of the polymer. This heightened viscosity may inhibit the growth of cells by hindering their expansion and coalescence, potentially leading to a denser foam rather than a lighter one. Consequently, while a low Te can be advantageous up to a certain point, it is of the utmost importance to optimize T_e rather than minimize it, in order to balance the effects of viscosity and pressure difference for the optimal foam density. This is similar to what happens in screw extruders for polymer foams [30,31]. The extrusion temperature has also a direct effect on the PBA expansion, as a higher temperature promotes a larger expansion, yet the inverse effect of T_e on the pressure difference is predominant on the direct one on the PBA expansion (see the blue symbols in 8d). It is also worth remarking that overcoming the melting temperature of the polymer can cause its degradation. On the other hand, the smaller T_e the larger the strand diameter, as shown by the SEM images in Figs. 8a–c and the red symbols in Fig. 8d. However, an extremely low T_e may lead to undesirable nozzle clogging. In addition, when T_e decreases, the polymer viscosity increases significantly: especially when coupled with a high extrusion speed, this can lead to adverse effects such as filament buckling or gear slippage, ultimately impeding the smooth flow of the material through the nozzle [32]. Finally, Fig. 8e shows the ABD radial distributions at the three T_e-values considered in the experiments. At the lowest T_e = 120 °C, the ABD is almost constant along the radius of the strand, however at larger T_e, the bubble size significantly increases towards the strand boundary. This is due to the fact that the outer part of the filament is in contact with the extruder hot wall, thus, the larger such temperature the more the peripheral bubbles are pushed to grow [33–35].

4.5. Speed of extrusion (S_e)

In the FAM technology, as well as in the MEX, the polymer filament flows through the hot end of the extruder with a velocity equal to S_e: since the PLA viscosity depends on the shear rate, the rheological

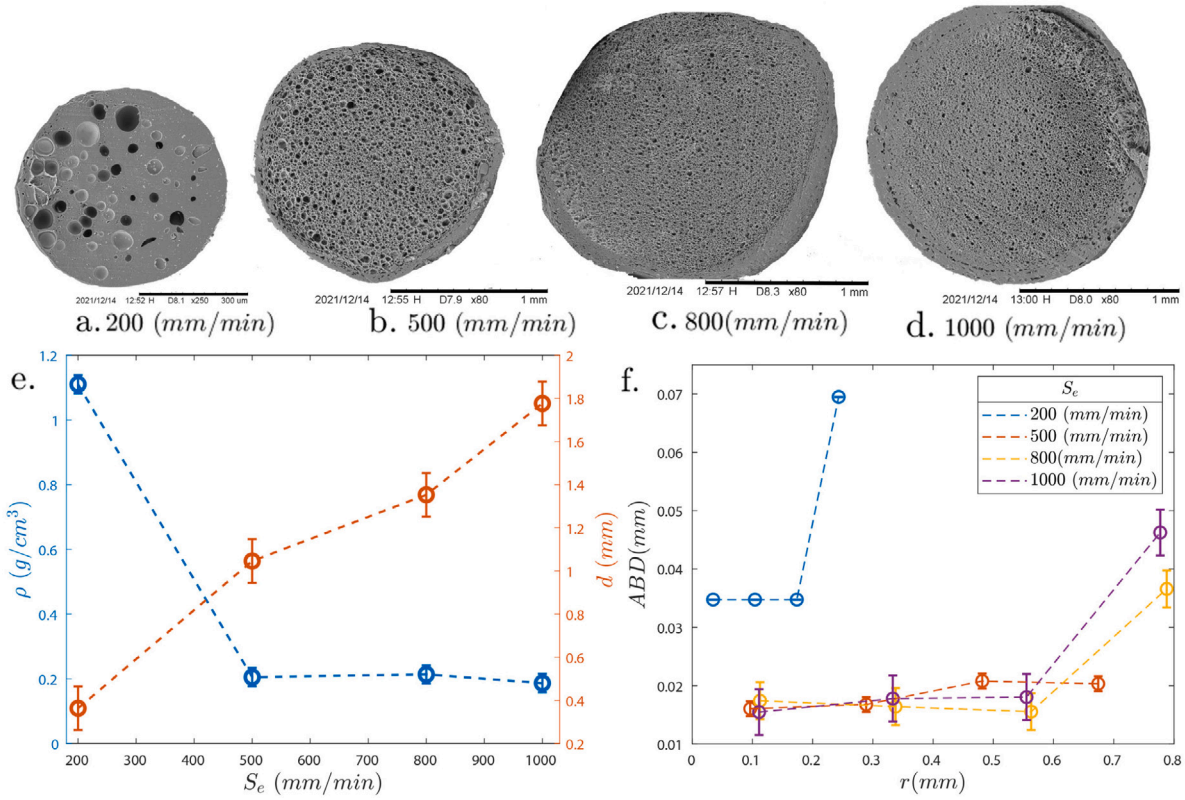

Fig. 9. SEM images of the cross section of strands obtained at P_a = 55 bar, t_a = 65 h, t_d = 24 h, T_e = 180 °C, D_n = 0.6 mm, and S_e = 200 (a), 500 (b), 800 (c), and 1000 (d) mm min^{-1}. e: Strand density (blue symbols, see the vertical axis on the left) and diameter (red symbols, see the vertical axis on the right) as a function of the speed of extrusion. f: Average bubble dimension along the radius of the strand at the four values of the extrusion speed considered in the experiments (see legend). In panels e–f, each point is obtained as the average of three measurements; the lines have the scope of guiding the eye. (For interpretation of the references to color in this figure legend, the reader is referred to the web version of this article.)

behavior of the polymer in the nozzle depends on S_e [6]. Given the geometry of the nozzle and the extrusion temperature, the pressure of the polymer in the nozzle increases with S_e [36], thus, as the pressure drop between inside and outside of the nozzle increases, the PBA expansion increases, so the polymer foaming is promoted [1]. From a macroscopic point of view, increasing S_e makes the diameter of the strand increase and the density decrease, as it can be observed by looking at the SEM images in Figs. 9a–d and the plots in Fig. 9e. In particular, at S_e = 200 mm min^{-1}, the strand density is 1.1 g cm^{-3} (close to that of pure PLA, equal to 1.25 g cm^{-3}) and the diameter of the strand is 0.4 mm, thus equal to $2/3D_n$, whereas, at S_e = 500 mm min^{-1}, the density drops to 0.2 g cm^{-3}; as S_e is further increased to 800 and 1000 mm min^{-1}, the density almost do not change, whereas the diameter increases until reaching 1.8 mm, corresponding to $3D_n$. Regrading the ABD, Figs. 9a and 9f show that, at S_e = 200 mm min^{-1}, the strand has few bubbles with an average size of 0.04 mm, whereas, when S_e is increased to 500 mm min^{-1}, the ABD substantially halves, with no relevant changes if S_e is further increased (except in the very outer part of the strand). This is a relevant result: indeed, if, for instance, the ABD corresponding to S_e = 1000 mm min^{-1} is desired, but such printing speed cannot be technologically reached, a comparable foam structure can be effectively produced even by operating at a reduced printing speed of 800 mm min^{-1}.

4.6. Nozzle diameter (D_n)

Given the extrusion speed, the diameter of the nozzle affects the flow rate of the polymer in the printer, thereby impacting the foam morphology. A larger D_n allows for a higher flow rate, leading to faster foam formation, larger cell size, yet lower foam quality. Conversely, a smaller nozzle diameter enables a finer control over the material flow, allowing for the production of foams with smaller cell size and improved resolution [37]. In addition, increasing D_n makes the pressure of the polymer in the nozzle decrease, thus hindering the strand expansion. Figs. 10a–c and 10d show that the strand diameter monotonically increases with the nozzle diameter (quite obviously), yet the density has a non-monotonic trend, attaining a minimum at D_n = 0.6 mm. On the other hand, if the expansion of the strand is evaluated relatively to the nozzle diameter, the strand diameter is equal to $3.5D_n$ at D_n = 0.4 mm, whereas it lowers to $2.75D_n$ at D_n = 0.8 mm. Finally, Fig. 10e shows that D_n does not have a significant quantitative influence on the ABD.

5. Discussion

The results presented in this work elucidate the nuanced effects of the process parameters on the foam morphology during the additive manufacturing process. This discussion aims to distil these findings into actionable insights that can directly inform those interested in producing foam products via MEX. The following section presents a list of parameters and a summary of their influence on foam morphology:

- **Pressure of Absorption** (P_a): Increasing the absorption pressure generally decreases the foam density and influences the concentration of blowing agents in the polymer.
- **Time of Absorption** (t_a): Longer absorption times allow for a more uniform distribution of bubbles, while shorter times create bubbles only in the outer area of the filaments.
- **Time of Desorption** (t_d): Extended desorption times can cause larger cells to form towards the external skin of the strand while maintaining smaller bubbles in the core, as it affects the concentration gradient of the blowing agent.

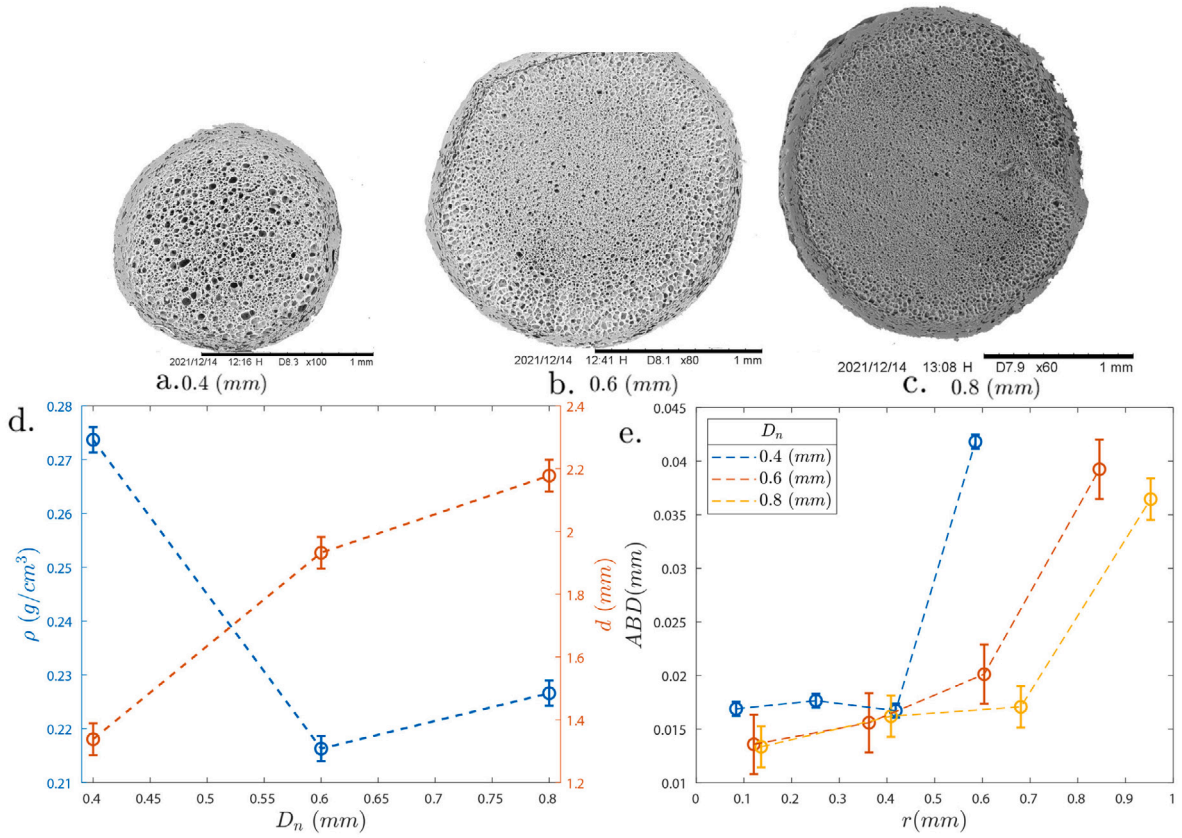

Fig. 10. SEM images of the cross section of strands obtained at P_a = 55 bar, t_a = 64 h, t_d = 24 h, T_e = 180 °C, S_e = 800 mm min^{-1}, and D_n = 0.4 (a), 0.6 (b), and 0.8 mm. d: Strand density (blue symbols, see the vertical axis on the left) and diameter (red symbols, see the vertical axis on the right) as a function of the nozzle diameter. e: Average bubble dimension along the radius of the strand at the three values of the nozzle diameter considered in the experiments (see legend). In panels d–e, each point is obtained as the average of three measurements; the lines have the scope of guiding the eye. (For interpretation of the references to color in this figure legend, the reader is referred to the web version of this article.)

- **Extrusion Temperature** (T_e): The temperature during extrusion plays a critical role in determining the viscosity of the polymer and the nucleation of bubbles, which are crucial for achieving desired foam expansion and density.
- **Extrusion Speed** (S_e): Faster extrusion speeds increase the shear rate and pressure drop, which can enhance the rate of cell nucleation and foam expansion, although excessively high speeds can lead to adverse effects such as filament buckling or gear slippage.
- **Nozzle Diameter** (D_n): The nozzle diameter mainly influences the final diameter of the filament, which during the printing process affects the resolution of the product.

The hexagonal plot presented in Fig. 11 offers a visualization of the influence of various process parameters on density and the diameter. Each vertex of the circle represents a distinct process parameter. The triangular points in red denote the minimum achievable values of each parameter when other parameters are held constant, providing insights into the lower bounds of material characteristics under specific conditions. The blue dotted line delineates the upper bounds of achievable outcomes, serving as a reference for maximum potential. The detailed analysis of process parameters presented in this study represents a significant advance in the field of additive manufacturing, particularly in the fabrication of bio-inspired structures. The capacity to tailor foam morphology through precise parameter control makes MEX systems especially well-suited for replicating the complex, hierarchical structures found in nature, such as bone matrices which require a delicate balance of strength and porosity. The study from Stano et al. [38], demonstrates the potential of MEX technology in the fabrication of rigid materials and silicone for applications that mimic biological tissues. The findings of this study contribute to the advancement of this emerging field by offering a systematic approach to fine-tune material properties for specific functionalities. This approach is instrumental for researchers and practitioners aiming to replicate the unique properties of biological structures in synthetic materials.

6. Conclusions

The research presented in this work sheds light on the effects of various process parameters on the outcomes of a foam additive manufacturing (FAM) process, in terms of foam morphology, average bubble dimension (ABD) distribution, and strand density and diameter.

This study identifies the speed of extrusion as a primary factor influencing the foam density. It also indicates that a high pressure of absorption (40 to 60 bar) does not significantly alter the foam density. A short time of absorption enables the bubbles to nucleate exclusively close to the external surface of the strands. The inverse influence of the time of desorption on bubble positioning within the strand cross section is also highlighted. The temperature of extrusion emerges as a pivotal factor affecting the foam properties, offering control over density and ABD. Finally, the nozzle diameter influences the strand diameter, although not directly affecting bubble size and distribution. This understanding enables informed process parameter selection and improves the possibility of predicting and engineering the final foam morphology to meet specific design requirements. Notably, a minimum density of 12.5% of the PLA bulk density was successfully attained.

The complexity of the relationships among the process parameters remains evident, underscoring the need for further research. Future investigations should delve deeper and possibly map interactions and cross-relations among those variables, to achieve even finer control over foam properties.

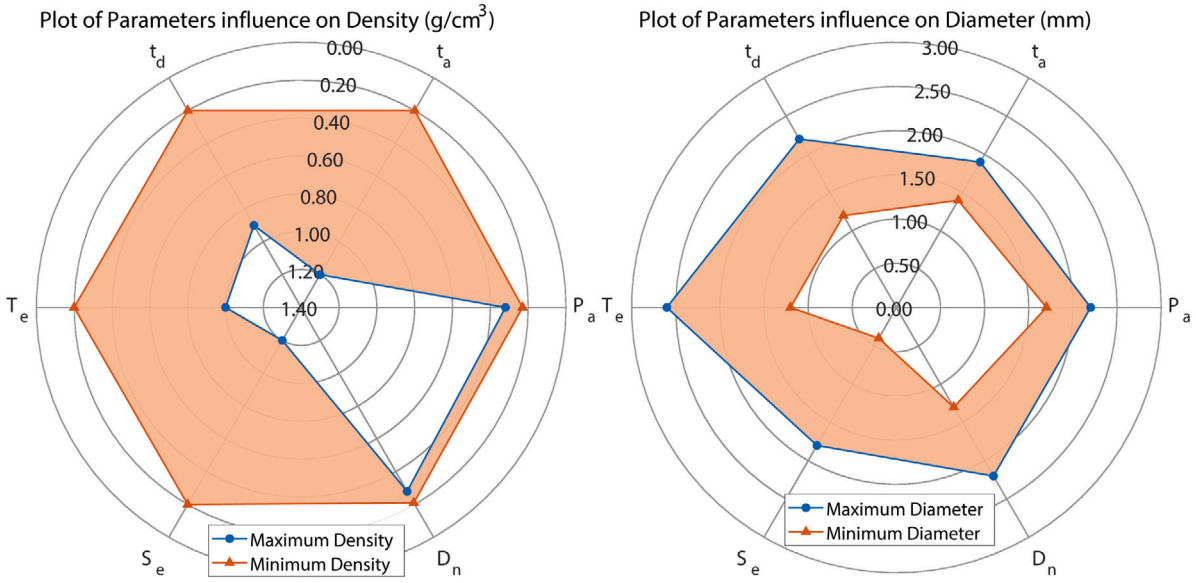

Fig. 11. Hexagonal Plot Illustrating Process Parameter Impact. Each angle of the circle corresponds to a process parameter, with the red triangular points representing minimum achievable values while fixing other parameters. The blue dotted line delineates the maximum achievable range, and the red area encompasses all possible combinations. (For interpretation of the references to color in this figure legend, the reader is referred to the web version of this article.)

CRediT authorship contribution statement

Andrea Lorenzo Henri Sergio Detry: Writing – review & editing, Writing – original draft, Visualization, Validation, Methodology, Investigation, Formal analysis, Data curation, Conceptualization. **Luca Landolfi:** Writing – review & editing, Writing – original draft, Visualization, Validation, Resources, Methodology, Investigation, Formal analysis, Data curation, Conceptualization. **Daniele Tammaro:** Writing – review & editing, Validation, Supervision, Formal analysis, Data curation, Conceptualization. **Antonio Lepore:** Writing – review & editing, Visualization, Investigation, Formal analysis, Data curation. **Massimiliano Maria Villone:** Writing – review & editing, Visualization, Investigation, Formal analysis, Data curation. **Pier Luca Maffettone:** Writing – review & editing, Supervision, Project administration, Conceptualization. **Antonino Squillace:** Writing – review & editing, Supervision, Project administration, Conceptualization.

Declaration of competing interest

The authors declare the following financial interests/personal relationships which may be considered as potential competing interests: Antonino Squillace reports financial support was provided by Italian Ministry of Research. If there are other authors, they declare that they have no known competing financial interests or personal relationships that could have appeared to influence the work reported in this paper.

Acknowledgment

This work was supported by the Italian Ministry of Research under the complementary actions to the NRRP "(Fir4MedRob - Fit for Medical Robotics)" Grant (#PNC0000007).

References

[1] Lee S-T. Foam extrusion : Principles and practice. 2000.
[2] Ambekar Rushikesh S, Kushwaha Brijesh, Sharma Pradeep, Bosia Federico, Fraldi Massimiliano, Pugno Nicola M, et al. Topologically engineered 3D printed architectures with superior mechanical strength. In: Materials today, vol. 48, Elsevier B.V.; 2021, p. 72–94.
[3] Perricone Valentina, Grun Tobias B, Rendina Francesco, Marmo Francesco, Candia Carnevali Maria Daniela, Kowalewski Michal, et al. Hexagonal voronoi pattern detected in the microstructural design of the echinoid skeleton. J R Soc Interface 2022;19(193):20220226.
[4] Reñones Patricia, Moya Alicia, Fresno Fernando, Collado Laura, Vilatela Juan J, de la Peña O'Shea Víctor A. Hierarchical TiO2 nanofibres as photocatalyst for CO2 reduction: Influence of morphology and phase composition on catalytic activity. J CO2 Util 2016;15:24–31, Special Issue on the XIII International Conference on Carbon Dioxide Utilization (ICCDU-2015).
[5] Chen Qiang, Pugno Nicola M. In-plane elastic buckling of hierarchical honeycomb materials. Eur J Mech A Solids 2012;34:120–9.
[6] Lombardi Lorenzo, Tammaro Daniele. Effect of polymer swell in extrusion foaming of low-density polyethylene. Phys Fluids 2021;33(3). 033104.
[7] Tammaro Daniele, Loianno Valerio, Errichiello Fabrizio, Di Maio Ernesto. Matricial foaming. Polym Test 2022;111:107590.
[8] Peng Fang, Vogt Bryan D, Cakmak Miko. Complex flow and temperature history during melt extrusion in material extrusion additive manufacturing. Addit Manuf 2018;22:197–206.
[9] Kwon Dong Eui, Park Byung Kyu, Lee Youn-Woo. Solid-state foaming of acrylonitrile-butadiene-styrene/recycled polyethylene terephthalate using carbon dioxide as a blowing agent. Polymers 2019;11(2).
[10] Nofar Mohammadreza, Utz Julia, Geis Nico, Altstädt Volker, Ruckdäschel Holger. Foam 3D printing of thermoplastics: A symbiosis of additive manufacturing and foaming technology. Adv Sci 2022;9(11):2105701.
[11] Thomas Tony, Zhang Cheng, Feliciano Ruiz Kristal M, Ramos-Pagan Carolina I, Ramos Negron Dariana M, Boesl Benjamin, et al. Engineering graphene-ceramic 3D composite foams by freeze drying. Adv Energy Mater 2021;23(7).
[12] Jiang Jungang, Oguzlu Hale, Jiang Feng. 3D printing of lightweight, super-strong yet flexible all-cellulose structure. Chem Eng J 2021;405:126668.
[13] Tammaro Daniele, Della Gatta Roberta, Villone Massimiliano Maria, Maffettone Pier Luca. Continuous 3D printing of hierarchically structured microfoamed objects. Adv Energy Mater 2022;24(5):2101226.
[14] Longo Alessandra, Giannetti Deborah, Tammaro Daniele, Costanzo Salvatore, Di Maio Ernesto. TPU-based porous heterostructures by combined techniques. Int Polym Process 2022;37(4):415–26.
[15] Kalia Karun, Ameli Amir. Understanding the process-microstructure-property relationships in material extrusion additive manufacturing of polylactic acid microcellular foams. Addit Manuf 2023;72:103636.
[16] Kalia Karun, Ameli Amir. Additive manufacturing of functionally graded foams: Material extrusion process design, part design, and mechanical testing. Addit Manuf 2024;79:103945.
[17] Flagiello D, Tammaro D, Erto A, Maffettone PL, Lancia A, Di Natale F. Foamed structured packing for mass-transfer equipment produced by an innovative 3D printing technology. Chem Eng Sci 2022;260:117853.
[18] Bonthu Dileep, Bharath HS, Gururaja Suhasini, Prabhakar Pavana, Doddamani Mrityunjay. 3D printing of syntactic foam cored sandwich composite. Compos Part C: Open Access 2020;3:100068.
[19] Visser Claas Willem, Amato Dahlia N, Mueller Jochen, Lewis Jennifer A. Architected polymer foams via direct bubble writing. Adv Mater 2019;31(46):1904668.
[20] Wirth David M, Jaquez Anna, Gandarilla Sofia, Hochberg Justin D, Church Derek C, Pokorski Jonathan K. Highly expandable foam for lithographic 3D printing. ACS Appl Mater Interf 2020;12(16):19033–43.

[21] Paquet Elodie, Bernard Alain, Furet Benoit, Garnier Sébastien, Le Loch Sébastien. Foam additive manufacturing technology: Main characteristics and experiments for hull mold manufacturing. Rapid Prototyp J 2021;27(8):1489–500.
[22] Tammaro Daniele, Detry Andrea Lorenzo Henry, Landonfi Luca, Napolitano Francesco, Villone Massimiliano Maria, Maffettone Pier Luca, et al. Bio-lightweight structures by 3D foam printing. In: 2021 IEEE 6th international forum on research and technology for society and industry. IEEE; 2021, p. 47–51.
[23] Tammaro D, Contaldi V, Carbone MG Pastore, Di Maio E, Iannace S. A novel lab-scale batch foaming equipment: The mini-batch. J Cellular Plastics 2016;52(5):533–43.
[24] Åström Karl J(Karl Johan). PID controllers. 2nd ed.. Research Triangle Park, N.C.: International Society for Measurement and Control; 1995.
[25] Tammaro Daniele, Villone Massimiliano Maria, Maffettone Pier Luca. Micro-foamed strands by 3D foam printing. Polymers 2022;14(15).
[26] Chen Lee, Sheth Himanshu, Kim Roland. Gas absorption with filled polymer systems. Polym Eng Sci 2001;41(6):990–7.
[27] Crank John. The mathematics of diffusion. Oxford University Press; 1979.
[28] Goel Satish K, Beckman Eric J. Generation of microcellular polymeric foams using supercritical carbon dioxide. I: Effect of pressure and temperature on nucleation. Polym Eng Sci 1994;34(14):1137–47.
[29] Chen Z-L, Chao P-Y, Chiu S-H. Proposal of an empirical viscosity model for quality control in the polymer extrusion process. Polym Test 2003;22(5):601–7.
[30] Naguib Hani E, Park Chul B, Reichelt N. Fundamental foaming mechanisms governing the volume expansion of extruded polypropylene foams. J Appl Polym Sci 2004;91(4):2661–8.
[31] Sauceau Martial, Fages Jacques, Common Audrey, Nikitine Clémence, Rodier Elisabeth. New challenges in polymer foaming: A review of extrusion processes assisted by supercritical carbon dioxide. Prog Polym Sci 2011;36(6):749–66.
[32] Gilmer Eric L, Miller Darren, Chatham Camden A, Zawaski Callie, Fallon Jacob J, Pekkanen Allison, et al. Model analysis of feedstock behavior in fused filament fabrication: Enabling rapid materials screening. Polymer 2018;152:51–61, SI: Advanced Polymers for 3DPrinting/Additive Manufacturing.
[33] Zhang Jie, Meng Fankai, Ferraris Eleonora. Temperature gradient at the nozzle outlet in material extrusion additive manufacturing with thermoplastic filament. Addit Manuf 2023;73:103660.
[34] Xia Huanxiong, Lu Jiacai, Tryggvason Gretar. A numerical study of the effect of viscoelastic stresses in fused filament fabrication. Comput Methods Appl Mech Engrg 2019;346:242–59.
[35] Xu D, Agassant J-F, Pigeonneau F. Dimensions of the deposited strand in the material extrusion process: Experimental and numerical investigations. Addit Manuf 2022;59:103107.
[36] Osswald Tim A, Puentes John, Kattinger Julian. Fused filament fabrication melting model. Addit Manuf 2018;22:51–9.
[37] Muñoz Jesús, Caminero Miguel, López Pedro, García-Plaza Eustaquio, Bécar Jean-Paul. Effect of nozzle diameter on mechanical and geometric performance of 3D printed carbon fibre-reinforced composites manufactured by fused filament fabrication. Rapid Prototyp J 2021;ahead-of-print.
[38] Stano G, Pricci A, Pavone A, Percoco G. Electromagnetic assistance enables 3D printing of silicone-based thin-walled bioinspired soft robots. Addit Manuf 2024;81:104028.